ACS OMEGA

Open Access

http://pubs.acs.org/journal/acsodf

Article

A New, Rapid, Colorimetric Chemodosimeter, 4-(Pyrrol-1-yl)pyridine, for Nitrite Detection in Aqueous Solution

Mallory E. Thomas, Lynn D. Schmitt, and Alistair J. Lees*

Cite This: *ACS Omega* 2024, 9, 37278−37287

Read Online

ACCESS | Metrics & More | Article Recommendations | Supporting Information

ABSTRACT: With increasing concerns over environmental impact and overall health of both the environment and its people, a need to quantify contaminants is of the utmost importance. Chemosensors with low detection limits and a relative ease of application can address this challenge. Nitrite ions are known to be detrimental to both the environment and human health. A new colorimetric chemodosimeter has been prepared from the homolytic photochemical cleavage of a reaction between pyrrole and pyridine. The product, 4-(pyrrol-1-yl)pyridine, yields a limit of detection of 0.330 (±0.09) ppm for the detection of nitrite in aqueous solution, employing a colorimetric change from yellow to pink. It is also highly selective for nitrite when various competitive anions such as SO_3^{2-}, NO_3^-, PO_4^{3-}, SO_4^{-2}, Cl^-, F^-, I^-, Br^-, AcO^-, and CN^- are present in great excess. The molecule's especially high sensitivity to nitrite is apparently the result of a complex supramolecular mechanism, characterized by both dynamic light scattering of the aggregate and the Tyndall effect. Consequently, this new sensor provides a simple, low-cost way to rapidly detect nitrite anions in aqueous solution.

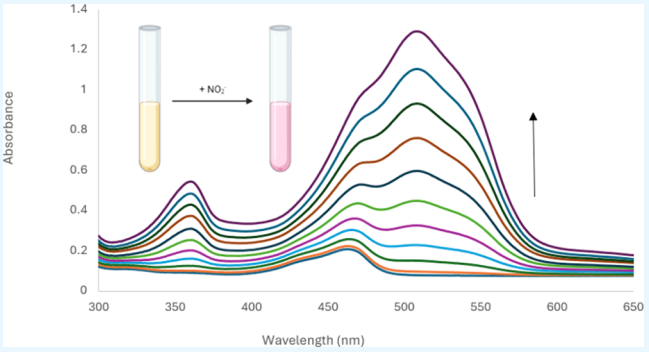

INTRODUCTION

As key components of the nitrogen cycle, nitrate and nitrite are commonly found infiltrated into both surface and groundwater systems. This is primarily due to contamination by animal waste and fertilizer or as a result of agricultural runoff.[1−5] The maximum contaminant level (MCL) of nitrite set by the U.S. Environmental Protection Agency (EPA) is 1 ppm.[1] Its high water solubility, in tandem with the low retention capability by soil, makes entryway in water systems easier.[6] However, its heightened ubiquity in water systems contributes to detrimental effects on aquatic ecosystems. Its environmental impact is attributed to anthropogenic nutrient pollution, which ultimately leads to eutrophication and can prove disastrous for aquatic ecosystems.[7−10] Additionally, the increased usage of nitrite in other capacities such as additives in the food industry, preservative science, and agriculture has resulted in overall elevated nitrite concentrations.[5,11,12]

Trace amounts of nitrites pose a risk to human health. They are considered type A inorganic chemicals, which require detailed monitoring due to their potential risks.[13,14] The World Health Organization (WHO) has enforced a limit of 3 ppm of nitrite in drinking water.[5] Typically, nitrite is found in consumer goods, such as beets, lettuce, and meat. Once combined with salt, it is thought to be the curing component that preserves food and provides the iconic pinkish color and fresh flavor of meat products.[15−19] While nitrites are primarily obtained through a diet of vegetables and cured meat, small amounts are also found in fish and dairy products. Here, meat products typically contain <0.2−6.4 mg of nitrite per kilogram, while dairy products contain <0.2−1.7 mg of nitrite per kilogram.[5] The presence of nitrite in consumer goods serves to prevent the growth of bacteria that can cause botulism disease.[20,21] However, its use as a preservative has been shown to have a probable connection between colorectal and stomach cancers in those with a high intake of cured meat.[22] Even those aforementioned trace amounts of nitrite ions are hazardous to human health. Nitrite-contaminated water has even caused shortness of breath and blue baby syndrome in infants once digested.[1,3,14] In the body, nitrite can interact with hemoglobin to form methemoglobin, where iron is oxidized to Fe^{3+}. Here, hemoglobin loses the ability to carry and release oxygen throughout the body and can cause hypoxia, most notably to the central nervous system.[5,23,24] Nitrite also plays a key role in human physiology as a signaling component.[25] However, after interacting with proteins, nitrites play a role in the generation of carcinogenic N-nitrosamines,[26] which can lead to gastric cancer.[27−30] Common symptoms can include cardiac dysrhythmias, mild dizziness, lethargy, and be as dire as a coma or

Received: May 28, 2024
Revised: July 16, 2024
Accepted: July 19, 2024
Published: August 20, 2024

convulsions.[31] It is also suggested that it is an indicator of bacterial contamination.[32] In addition, an elevated risk of non-Hodgkin's lymphoma has been reported.[33] It has previously been reported that concentrations ranging from 33 to 250 mg of nitrite per kg of body weight is lethal, with 0.4−200 mg/kg of body weight enough to cause methemoglobinemia.[34]

Common detection methods for nitrite employ electrochemical methods,[35,36] fluorescence spectroscopy,[37−40] UV−visible spectroscopy,[39] chemiluminescence,[41,42] chromatography, and flow injection analysis.[43] However, many of these methods are susceptible to interference from other particles in water, have high cost and need sophisticated equipment, are exceedingly complicated with intricate experimental steps, and consume high amounts of materials. Nitrite also has the potential to be indirectly detected in colorimetric assays that employ a diazotization reaction between nitrite and sulfanilamide, but these are prone to interference from other agents.[44−46] To alleviate these challenges, there is a priority for the development of sensors with increased sensitivity, selectivity, lower cost, and increased ease of portability. From this, a large variety of compounds have been employed to create nitrite sensors such as nanoparticles,[35] metal oxides, carbon materials,[36,47] and other organic frameworks.[40] However, colorimetric methods are still the most highly sought after for their portability, simplicity, and the rapid response seen with the naked eye.[48,49] A review by Singh et al. thoroughly illustrates the large range of detection limits, advantages, and challenges various methods of nitrite detection face.[50] Here, listed limits of detection for nitrite range from approximately 1.2×10^{-6} to 1.2 ppb. Even within colorimetric sensors, current systems report reaction wait times of 15 min for results[46] and pH dependency as the most common factors.[45,48,50] Here, we offer a new colorimetric organic chemodosimeter, 4-(pyrrol-1-yl)pyridine, that reveals both high sensitivity and selectivity to nitrite in aqueous solutions. Its rapid response and detection limit of 0.330 (±0.09) mg/L offer a solution to the need for low-cost, simpler, portable, and efficient nitrite sensors.

MATERIALS AND METHODS

Reagents. All materials were purchased commercially and used as received, unless specified. The following materials were used: methylene chloride (Fisher, 99%), pyrrole (Fisher, 99%), 4-chloropyridine hydrochloride (Sigma, 99%), hydrochloric acid (Fisher, 98%), sodium carbonate (Fisher, 99%), anhydrous sodium sulfate (Fisher, 99%), sodium nitrate (Fisher, 99%), sodium nitrite (Fisher, 99%), sodium phosphate (Fisher, 99%), sodium chloride (Fisher, 99%), sodium fluoride (Fisher, 99%), sodium bromide (Fisher, 99%), potassium iodide (Fisher, 99%), potassium cyanide (Fisher, 99%), sodium acetate (Fisher, 99%), dimethyl sulfoxide (Fisher, 99%), chloroform (Fisher, 99%), acetonitrile (Fisher, 99%), acetone (Fisher, 99%), diethyl ether (Fisher, 99%), and hexane (Fisher, 99%). Spectroscopy grade 18 MΩ water was used as the solvent, unless otherwise specified.

Synthesis of 4-(Pyrrol-1-yl)pyridine. Synthesis of 4-(pyrrol-1-yl)pyridine was carried out using an analogous photochemical procedure for a related compound previously published by Seki et al.[51,52] The synthesis of 4-(pyrrol-1-yl)pyridine was carried out in a 1:32 ratio of 4-chloropyridine hydrochloride (0.001 mol) to freshly distilled pyrrole (0.032 mol). In a 250 mL quartz round-bottom flask, 4-chloropyridine hydrochloride (0.150 g) was dissolved in methylene chloride (100 mL) and allowed to stir under bubbling of nitrogen gas for 1 h. Pyrrole (2.22 mL) was added, and the mixture was irradiated for 6 min while stirring under a constant flow of nitrogen. Typically, after 1 min, the solution begins to turn yellow and continues to deepen in color throughout photolysis. The reaction was monitored via UV−visible spectroscopy and NMR analysis to reveal no unwanted side products in the solution. The 1:32 ratio of 4-chloropyridine to pyrrole was found to be optimum; an excess of pyrrole is required to avoid bipyridine formation. Post synthesis analysis identified only unreacted starting material in addition to the product, where the former is removed during the extraction process. This synthetic procedure was carried out in additional solvents (ethanol and hexane) but exhibited the same results. However, prolonged light exposure after 20 min leads to the formation of insoluble black polypyrrole side products.

Polypyrrole formation does not significantly affect the overall yield of the reaction, and it appears as a film on the surface of the reaction mixture; it can be easily isolated and removed via filtration of the reaction mixture before the extraction process. The reaction is monitored via UV−visible spectroscopy until completion. Here, the formation of a visible band maximum at 463 nm forms over the course of the reaction. As previously mentioned, prolonged light exposure causes the formation of polypyrrole. After 6−12 min of irradiation, an absorbance maximum starts to appear at 574 nm, giving the first indication of polypyrrole side product. Therefore, an irradiation time of no longer than 12 min was employed to minimize this effect.

The product, 4-(pyrrol-1-yl)pyridine, was extracted with three washes of 10% hydrochloric acid in a volume of 30 mL total. The aqueous layer was separated and neutralized using solid sodium carbonate until a neutral pH was reached, and the contents were measured via a pH probe. The neutralized aqueous layer was extracted with four washes of dichloromethane for a volume of 20 mL total to remove any excess pyrrole and other organic impurities. The resulting yellow-orange organic solution was dried via solid anhydrous sodium sulfate and decanted, and the liquid was subsequently concentrated to dryness to yield a brown oil, resulting in yields up to 65%. The resulting product was stored at 277 K to aid in its preservation. IR spectra indicate all expected functional groups, and the mass spectrum reveals the parent ion (M^+: 146 m/z). Spectroscopic studies of oil stored for upward of six months showed no structural degradation, as measured by NMR and UV−visible spectroscopy.

Instrumentation and Procedures. All aqueous solutions were filtered prior to use. UV−visible spectra were taken on a Shimadzu UV−vis spectrometer in spectroscopy grade 18 MΩ water unless otherwise stated. Spectra were recorded at 303 K in a 1.00 cm path length quartz cuvette, and baselines were set with 18 MΩ water as a reference, unless indicated otherwise. An Oriel Mercury/Xenon medium pressure lamp (200 W) was used for the photochemical synthesis of 4-(pyrrol-1-yl)-pyridine. All NMR data were recorded on a Bruker NEO 400 MHz spectrometer in 99.9% pure $CDCl_3$, 99% pure D_2O, or 99% pure *d*-DMSO, and high precision 535-pp NMR tubes were used. Dynamic light scattering (DLS) data were obtained using a Malvern Zetasizer Lab using 18 MΩ water as a solvent at room temperature in Malvern Zetasizer nano series plastic cuvettes. The volumes used matched the minimum volume of the instrument, being approximately 1 mL. The refractive index used was 1.59. Five duplicates were obtained with an

https://doi.org/10.1021/acsomega.4c05026
ACS Omega 2024, 9, 37278−37287

equilibrium time of 20 s using a side scatter angle of detection. Fluorescence spectroscopy was performed on a Horiba Jobin FluoroMax 3 fluorescence spectrometer with excitation wavelengths between 340 and 460 nm. Fluorescence cuvettes were used for all spectra with a 1 cm path length. FT-IR spectroscopy was recorded on a Shimadzu FT-IR instrument fitted with a liquid cell made of a NaCl aperture plate. LC-MS data were obtained using a Shimadzu LC-MS-2020 with a quadrupole. Solutions were prepared at a concentration of 2 mg/mL and filtered after dissolution in LC-MS grade water. A C18 column was employed with a column eluent of water (0.1% formic acid) and acetonitrile (0.1% formic acid) in the positive channel.

Titration with 1.00 × 10^{-2} M Sodium Nitrite (aq). All aqueous solutions of 4-(pyrrol-1-yl)pyridine were recorded immediately after dissolution in 18 MΩ water to avoid thermal degradation. A freshly prepared solution of 4-(pyrrol-1-yl)pyridine was made in 18 MΩ water, and UV−visible spectra were recorded over the range of 200−800 nm. A sample of 1.00 × 10^{-2} M aqueous sodium nitrite was prepared in a 100.00 mL volumetric flask and mixed until homogeneous. Titrations of 2.00 μL (1.00 × 10^{-2} M) of sodium nitrite were injected into 2.00 mL of aqueous 4-(pyrrol-1-yl)pyridine via a micropipette. The subsequent spectra were monitored via UV−visible spectroscopy immediately upon addition of nitrite, and the colorimetric change from yellow to pink was also observed using the naked eye. Plots for the limit of detection determinations (LOD) used the starting absorbance at 509 nm of the sensor (A_{sensor}), absorbance upon each successive addition of nitrite at 509 nm ($A_{nitrite}$), maximum absorbance at 509 nm after all additions of nitrite (A_{max}), and minimum absorbance at 509 nm (A_{min}). Errors for the limit of detection values were obtained from the standard deviation of 10 measurements.

Competitive Anion Titrations. A freshly prepared solution of 4-(pyrrol-1-yl)pyridine was added to 18 MΩ water. Competitive anion solutions were made in 1:50 ratios (1.00 × 10^{-2} M nitrite, 0.5 M competing anion) in 100 mL volumetric flasks using their sodium or potassium salts. Solutions of 6.76 × 10^{-4} M 4-(pyrrol-1-yl)pyridine were titrated with 1.00 μL injections for a total of 4 additions (4.00 μL). Spectra upon each addition were monitored by UV−visible spectroscopy.

Dynamic Light Scattering. Approximately 1 mL of aqueous samples of 4-(pyrrol-1-yl)pyridine in 18 MΩ water were inserted into a plastic cuvette matching the required volume minimum of the instrument. Five trials were recorded per sample employing a refractive index of 1.59, equilibration time of 20 s, and a side scatter angle of detection.

Tyndall Effect. Approximately 4 mL aqueous samples of 4-(pyrrol-1-yl)pyridine were irradiated with light from a helium laser in a dark room to determine if light scattering was present.

RESULTS AND DISCUSSION

Synthesis and Characterization of 4-(Pyrrol-1-yl)-pyridine. The UV−visible spectra recorded during the synthesis of 4-(pyrrol-1-yl)pyridine in methylene chloride are shown in Figure 1. The photochemical reaction between pyrrole and pyridine appears to be clean and uncomplicated from side products for 20 min of irradiation. Prolonged light exposure beyond 20 min, however, leads to the formation of polypyrrole. The energy of irradiation due to the Hg/Xe lamp

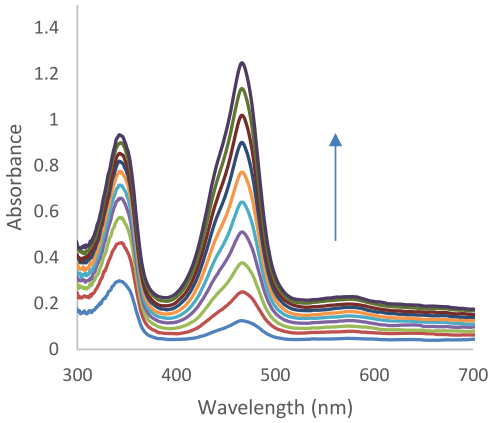

Figure 1. UV−visible difference spectra monitored during the synthesis of 4-(pyrrol-1-yl)pyridine in methylene chloride with readings every 2 min for a total of 20 min.

is sufficiently high in energy to cleave both the C−Cl bond of 4-chloropyridine (338.2 kJ/mol) and the N−H bond of pyrrole (351 kJ/mol).[53] Confirmation of the resulting product 4-(pyrrol-1-yl)pyridine (90 mM) via ^{1}H NMR in *d*-DMSO yields δ 8.56 (dd, *J* = 8 Hz, 2H), δ 7.55 (dd, *J* = 4 Hz, 2H), δ 6.73 (q, *J* = 2.16 Hz, 2H), and δ 6.01 (q, *J* = 2.1 Hz, 2H) with equal integrations. Additionally, ^{13}C NMR assignments further confirm the creation of 4-(pyrrol-1-yl)pyridine with the following chemical shifts: δ 151.6, δ 143.3, δ 124.6, δ 117.8, and δ 107.6 ppm. This was found to be similar to previously determined NMR positions accounting for $CDCl_3$ solvent[54−56] and matched the splitting pattern of the employed starting reagents with pyrrole peaks shifted upfield by approximately 0.2 ppm.[57] ^{1}H and ^{13}C NMR assignments obtained in *d*-DMSO are in accordance with the structure of 4-(pyrrol-1-yl)pyridine, as shown in Figure 2. Two-dimensional ^{1}H NMR

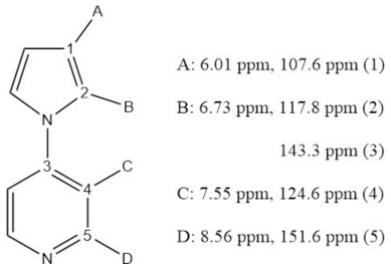

Figure 2. 4-(Pyrrol-1-yl)pyridine with ^{1}H and ^{13}C NMR assignments.

(COSY, HSQC) further confirms the 4-(pyrrol-1-yl)pyridine product by depicting H-bond interactions between the pyrrole hydrogens and the pyridine hydrogens on the molecule; see Supporting Information.

^{1}H NMR concentration studies of 4-(pyrrol-1-yl)pyridine were carried out in $CDCl_3$ to determine any changes in structural determination. A 30 mM sample of 4-(pyrrol-1-yl)pyridine yields sharp peaks with clear splitting and approximately equal integrations of 0.967, 0.974, 0.920, and 0.912, which is consistent with what is seen in *d*-DMSO. However, more concentrated samples of 4-(pyrrol-1-yl)-pyridine of 90 and 124 mM sensors in $CDCl_3$ depict shifting of both pyridine protons and significant peak broadening indicative of intermolecular interactions. Here, integrations were also approximately equal to one with the 90 mM 4-

https://doi.org/10.1021/acsomega.4c05026
ACS Omega 2024, 9, 37278−37287

(pyrrol-1-yl)pyridine spectra, having integrations of 1.00, 1.45, 1.61, and 1.62, and the 124 mM 4-(pyrrol-1-yl)pyridine spectra, yielding integrations of 1.00, 1.29, 1.40, and 1.40. Both can be found in the Supporting Information.

The product is yellow in color and exhibits both a band maximum at 463 nm and significant scattering at long wavelengths in the UV−visible spectrum, shown in Figure 3.

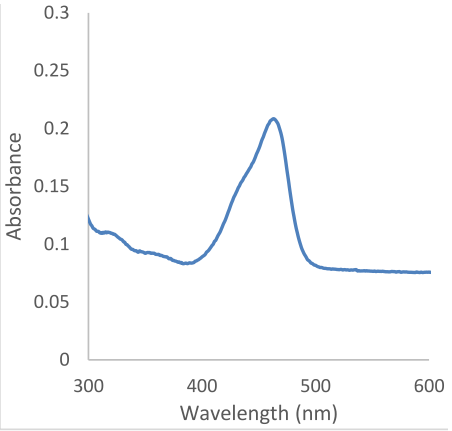

Figure 3. UV−visible spectrum of 4-(pyrrol-1-yl)pyridine (2.66×10^{-2} M) in 18 MΩ water. Baseline correction was against a blank of 18 MΩ water.

No emission was observed for this system. Dilutions of 4-(pyrrol-1-yl)pyridine depicted a molar absorptivity of 110 M^{-1} cm^{-1}. Solvent dependence was carried out using diethyl ether, chloroform, acetone, methanol, dimethyl sulfoxide, and water; a new visible band maxima was determined in all cases except water. Here, a new band at 500 nm began to form in all solvents, except water. These results illustrate a bathochromic shift with increasing solvent polarity, which is typical of a $\pi \rightarrow \pi^*$ transition. However, most spin-allowed $\pi \rightarrow \pi^*$ transitions normally yield larger molar absorptivity values; thus the electronic transition observed in this system is highly unusual, *vide infra*.

Anion Sensing by 4-(Pyrrol-1-yl)pyridine. The compound 4-(pyrrol-1-yl)pyridine was studied with various anions to determine its anion sensing properties. Upon the addition of aqueous sodium nitrite, the system showed a colorimetric change from yellow to pink with increasing absorbance upon each addition of nitrite. Figure 4 illustrates a titration recorded by acquiring the UV−visible spectra between the sensor, 4-(pyrrol-1-yl)pyridine, and the analyte, $NaNO_2$(aq). The observed band at 463 nm, indicative of the yellow starting sensor solution, undergoes a bathochromic shift, and new bands begin to appear at 360 and 509 nm, with the latter indicative of the pink final product in solution; see Figure 5.

While the large bathochromic shift of 1952 cm^{-1} is characteristic of this system, previous work has illustrated similar phenomena.[58−67] In most cases, the shift is indicative of changing intermolecular or intramolecular interactions in the system. Many systems using anion sensing show red shifting with interaction of anions based on either enhanced intermolecular charge transfer,[60] "long-range Coulombic coupling",[66] changes in the chromophore's geometry and orientation in solution through electrostatic interactions,[67] increased shielding of structural moieties of the sensor,[62] or even those with an anion concentration dependent red shift.[64] This is discussed in further detail below.

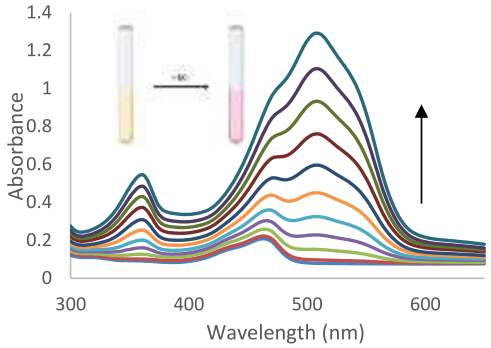

Figure 4. UV−visible spectra of a titration between 4-(pyrrol-1-yl)pyridine (1.89×10^{-3} M) in 18 MΩ water with increasing 2.00 μL additions of 1.00×10^{-2} M sodium nitrite (aq). Initial spectrum is before nitrite addition. Inset illustrates the colorimetric change upon addition of a nitrite ion.

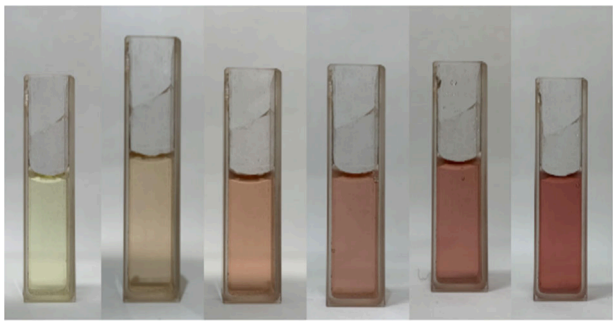

Figure 5. Color changes observed for a 2.15×10^3 M aqueous solution of 4-(pyrrol-1-yl)pyridine (2.0 mL) with 0.0, 20.0, 40.0, 60.0, 80.0, and 100.0 μL additions of 0.01 M sodium nitrite, left to right, respectively.

Each nitrite addition produced an instantaneous color change and was found to be irreversible over time. From these results, a LOD was determined for this sensor system, via a plot of the absorbance changes at 509 nm versus added sodium nitrite concentration; see Figure 6. The LOD was calculated via eq 1, where σ is the standard deviation of the blank, and s is the slope of the line generated.

$$\mathrm{LOD} = 3\sigma/s \quad (1)$$

A value of 0.330 (±0.09) ppm was subsequently obtained for these colorimetric changes in 4-(pyrrol-1-yl)pyridine upon addition of aqueous sodium nitrite, revealing a high sensitivity of the molecule to the added nitrite ion. This result was found to be consistent and unaffected by the initial sensor concentration.

The selectivity of this system was subsequently investigated by using a competitive anion study. Competing anions of sulfite, nitrate, phosphate, sulfate, chloride, fluoride, iodide, bromide, acetate, and cyanide were used in 50 molar equiv compared to nitrite. After a total of four 1.00 μL additions of each 1:50 aqueous solution, none displayed any affinity of competitiveness toward 4-(pyrrol-1-yl)pyridine. Additionally, in all cases, the color change to pink upon addition of nitrite was unaffected by the other anion being present and exhibited a minimum percent increase of 62% in the absorbance at 509 nm; see Figure 7. Therefore, the 4-(pyrrol-1-yl)pyridine system was found to be both highly sensitive and selective toward nitrite ions in aqueous solutions.

https://doi.org/10.1021/acsomega.4c05026
ACS Omega 2024, 9, 37278−37287

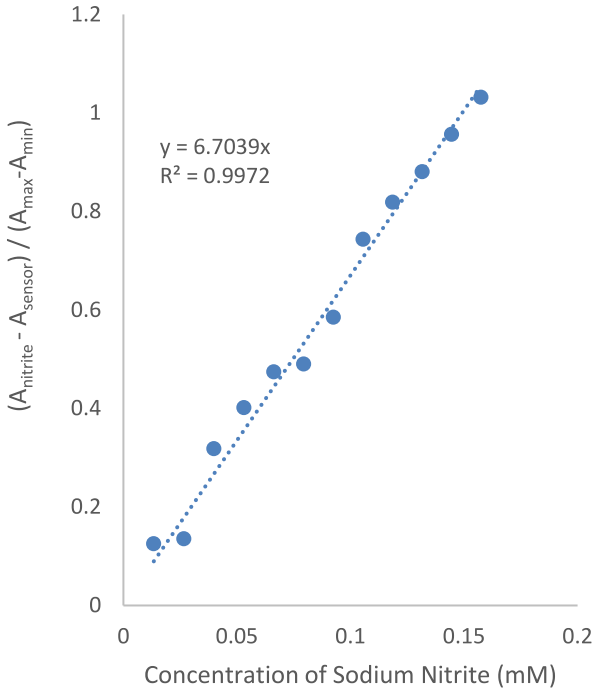

Figure 6. Limit of detection determination of 4-(pyrrol-1-yl)pyridine from a plot of absorbance changes at 509 nm on addition of sodium nitrite (aq) in 18 MΩ water.

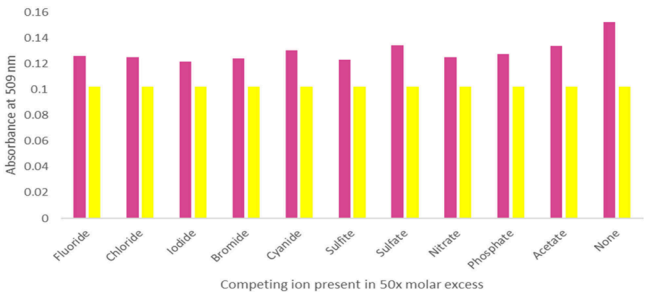

Figure 7. Absorbance at 509 nm of sensor solution (R, yellow) and sensor solution with a single 4.00 μL addition of 1.00×10^{-2} M nitrite and 0.5 M competing anion (L, pink) in 18 MΩ water.

These results were found to be consistent and reproducible in the pH range of 1−7. Carbonate anions were omitted from the competitive anion study due to their neutralization effect on the sensor. At basic pH, the sensor no longer interacts with nitrite anions. In addition, temperature dependence studies revealed the stability of the sensor system at room temperature for 24 h. Utilizing these reaction conditions, the sensor system was highly reproducible, producing LOD values in the stated range when in aqueous solution. Moreover, the extracted oil samples of 4-(pyrrol-1-yl)pyridine are stable stored at 277 K for up to 6 months.

Possible Mechanism of Sensing. Having established the irreversibility of the color change and both the high sensitivity and high selectivity of this system, the mechanism was further investigated. Spectroscopic changes observed in a single injection showed a more than 20% increase of absorbance at 509 nm. The nitrite concentration in solution (1.33×10^{-5} M) is much lower than that of the 4-(pyrrol-1-yl)pyridine sensor (2.51×10^{-3} M), illustrating the interaction here is not a simple 1:1 or 1:2 stoichiometry. NMR characterization of the final product proved to be problematic, though. It is common knowledge that pyrroles will react with nitro groups by irreversibly binding at the 2 position on the pyrrole ring.[55,56,68] Hence, it is hypothesized that a similar final product is formed through strong electrostatic interactions and not through formation of a covalent bond. The system, however, is complicated by what appears to be the formation of an aggregate. As noted above, the visible absorption band at 463 nm with low molar absorptivity is indicative of $\pi \rightarrow \pi^*$ transitions and π stacking. Moreover, there is a significant absorbance increase at 700 nm, indicative of substantial light scattering, providing further evidence that the product forms on a supramolecular scale.

The presence of an aggregate poses challenges in terms of characterization. It is common for aggregated systems to experience broadening of peaks in NMR analysis due to the many intra- and intermolecular forces in solution and even restricted rotation capabilities.[69−72] Previous studies have determined that NMR analysis of molecules dissolved in liquid crystalline phase is incredibly difficult to decipher due to the large number of spectral transitions present.[73] Raising the concentration of 4-(pyrrol-1-yl)pyridine in NMR analysis further broadened the peaks with increasing concentration of the sensor due to the increased presence of aggregates in solution and the many intermolecular interactions causing the pyridine proton signals to broaden; see Figure 8. The peak locations for both pyridine protons are as follows: δ 8.58 and δ 7.36 ppm for 120 mM in $CDCl_3$, δ 8.58 and δ 7.36 ppm for 90 mM in $CDCl_3$, δ 8.60 and δ 7.39 ppm for 60 mM in $CDCl_3$, and δ 8.56 and δ 7.52 ppm for 30 mM in $CDCl_3$.

Further support of intermolecular interactions in the sensor were studied comparing ^{1}H NMR spectra of samples with different solvents. Here, 120 mM solutions of 4-(pyrrol-1-yl)pyridine were made in both $CDCl_3$ and *d*-DMSO. It is observed that the broadening present in ^{1}H NMR of the pyridine hydrogens in the 4-(pyrrol-1-yl)pyridine system is consistent with intermolecular interactions when $CDCl_3$ is employed as the solvent. However, to confirm this, the same solution was analyzed in *d*-DMSO, a solvent known to disrupt intermolecular interactions. The lack of broadening seen with this solvent even at higher concentration is indicative of the breakdown of intermolecular forces holding the supramolecular system together; see Supporting Information. This supports the slight differences in NMR peak splitting from previous literature values, as both the concentration of the sample and the desired solvent can affect the spectra through peak shifting, broadening, and splitting.

Typically, highly conjugated systems exhibit broadening in their NMR spectra.[74] The broad components of an NMR spectrum appearing in the aromatic region are due to the formation of π stacking and arise from the perturbation of shielding effects with subsequent aromatic rings above or below in these supramolecular structures.[74] This is commonly termed the "ring current" effect of conjugated aggregate systems. Previous work illustrates this phenomenon with porphyrin systems where ring current effects cause a broadening in the NMR spectrum.[75] Additionally, it has been determined that multiple relaxation mechanisms in ^{1}H NMR can affect line widths and therefore are more prevalent in spectra of molecules that contain a quadrupolar nucleus, such as a pyridine moiety.[73]

In tandem with the line broadening, shifts in location of the aromatic protons are the result of delocalization of electrons from the ring current effect of the π stacking, causing a

https://doi.org/10.1021/acsomega.4c05026
ACS Omega 2024, 9, 37278−37287

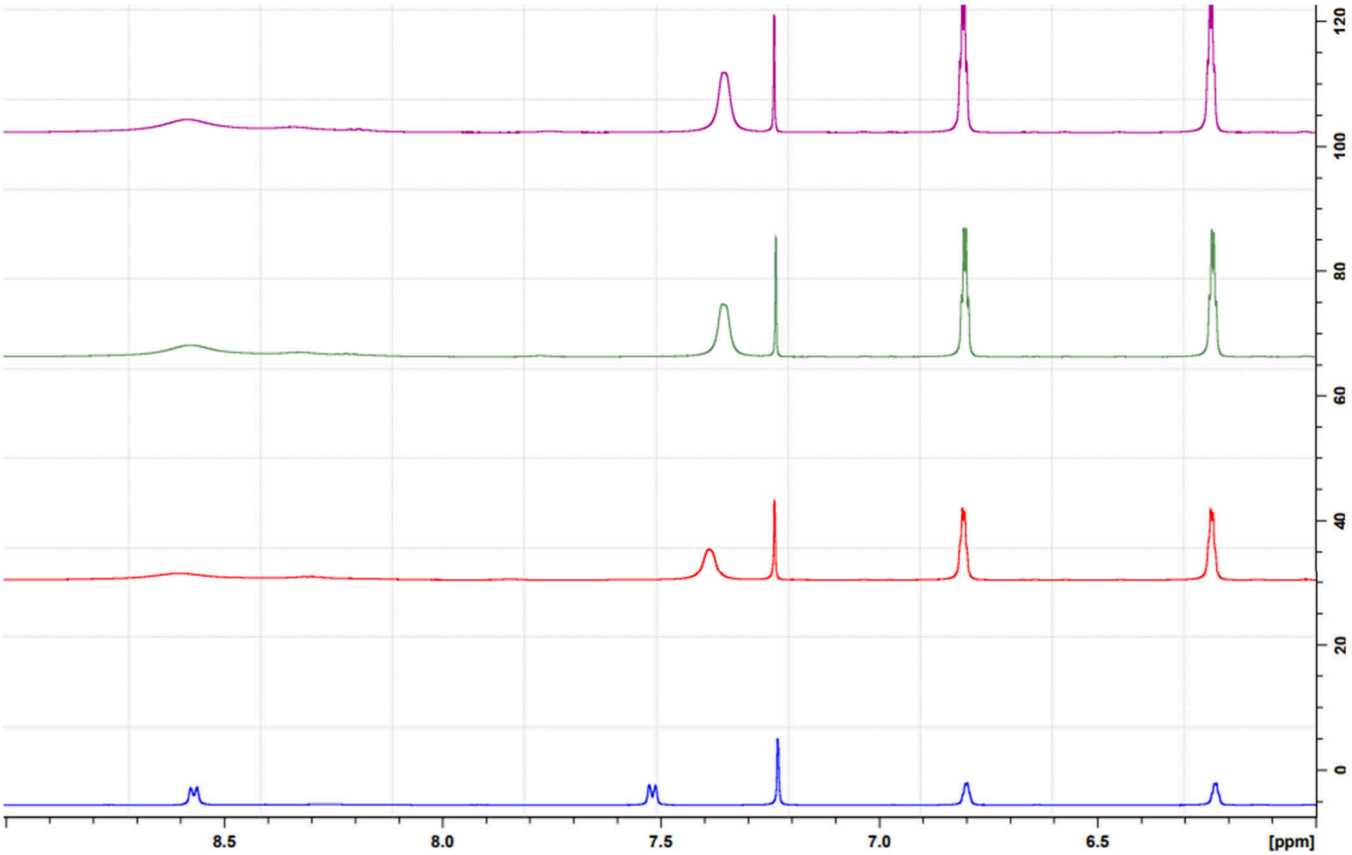

Figure 8. Proton NMR spectra of various concentrations of 4-(pyrrol-1-yl)pyridine in $CDCl_3$. Top to bottom: 120 mM, 90 mM, 60 mM, and 30 mM, respectively.

downfield shift.[74] Hence, the extent of aggregation and overall magnitude of the intermolecular interactions can cause nuclei to have resonances at various shifts.[75] We observed this in the NMR spectrum of the 90 mM sensor solution in $CDCl_3$, where signals from the pyridine ring were broadened significantly compared to that of a 30 mM solution. Furthermore, the 120 mM sensor solution in $CDCl_3$ exhibits an even larger extent of broadening with increased concentration.

Consequently, the product with the absorption maximum at 509 nm (sensor−nitrite adduct) would be anticipated to show peak broadening in its NMR. While we were unable to obtain full ^{13}C NMR characterization due to consistently increased baseline noise in the spectrum while utilizing D_2O/H_2O solvent, we believe the product is a large aggregate with a strong electrostatic interaction between nitrite and the pyrrole group of the 4-(pyrrol-1-yl)pyridine system and not the formation of a covalent bond. This would be similar to nitro-pyrrole-based moieties that yield the following shifts in D_2O/H_2O: δ 8.65 (d, J = 4 Hz, 2H), δ 8.06 (d, J = 4 Hz, 2H), δ 6.81 (s, 2H), and δ 6.14 (s, 2H) with an approximately 1:10 integration of the pyridine to pyrrole hydrogens; see Supporting Information. Here, the broadening of only the pyrrole peaks to singlets further supports the increased intermolecular attraction between nitrite and the pyrrole moiety of the 4-(pyrrol-1-yl)pyridine system. Additionally, all peaks exhibit a downfield shift due to the intermolecular interaction with nitrite. Two-dimensional COSY NMR revealed that both pyrrole peaks (δ 6.81 and δ 6.14) no longer couple with each other. This loss in adjacent proton coupling further corroborates the electrostatic interaction of 4-(pyrrol-1-yl)pyridine with nitrite on the pyrrole ring; see Supporting Information.

A quick qualitative test for aggregates in solution is done by employing the Tyndall effect.[76−79] Figure 9 depicts the Tyndall effect in the sensor sample compared to that in 18 MΩ water, filtered prior to use.

Here, light is scattered if a colloid is present, where it is large enough to carry the light through solution; a true solution, like 18 MΩ water, would have no colloids present to scatter the

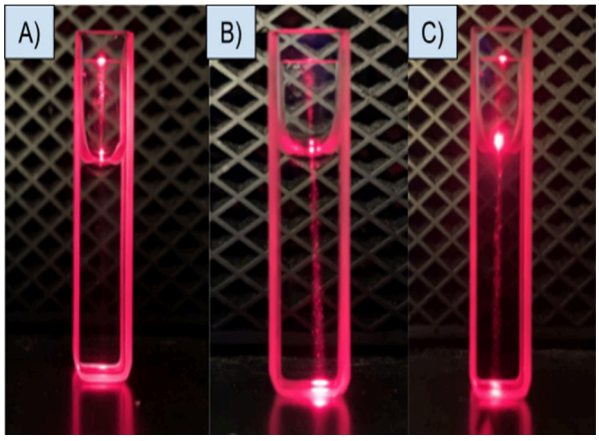

Figure 9. Depiction of the Tyndall effect: (A) 18 MΩ water with no light scattering observable, (B) 4-(pyrrol-1-yl)pyridine with light scattering shown in 18 MΩ water, and (C) 4-(pyrrol-1-yl)pyridine and nitrite final product with light scattering shown in 18 MΩ water.

https://doi.org/10.1021/acsomega.4c05026
ACS Omega 2024, 9, 37278−37287

light. Through the use of the Tyndall effect, light was scattered through a solution of 4-(pyrrol-1-yl)pyridine, confirming the presence of an aggregated species.

To provide an estimate on the extent of aggregation, DLS is commonly employed to determine a rough estimate of particle size of aggregates or nanoparticles.[79,80] After analysis of aqueous samples of 4-(pyrrol-1-yl)pyridine using DLS, an estimate of aggregate size was obtained over a range of concentrations, each with five duplicate trials, as shown in Table 1. The size was determined using the weighted averages of the DLS values obtained.

Table 1. DLS Aggregate Size over a Range of Concentrations of Aqueous 4-(Pyrrol-1-yl)pyridine

Concentration (M)	Absorbance at 463 nm	Size (nm)
7.20×10^{-3}	0.792	363
6.50×10^{-3}	0.715	249
3.68×10^{-3}	0.405	195
2.11×10^{-3}	0.232	142

Here, it is important to consider that highly aromatic systems have a propensity to aggregate in solution.[81−86] Specifically, conjugated systems, like heterocycles pyridine and pyrrole, have been seen to form aggregates through π-stacking interactions.[87−89] Within this, however, different forms can appear with various π-stacking aggregate conformations.[89] It has been reported that when two aromatic moieties absorb in the ultraviolet region of the electromagnetic spectrum, after combining, the newly formed aggregate is likely to absorb in the visible region.[89] This serves to further support an aggregated system between our two aromatic UV absorbing moieties reacting to form a new aggregate absorbing in the visible region (463 nm). In addition, the system does not exhibit fluorescence, providing no indication of the formation of an excimer. Hunter and Sanders reported four rules with respect to π-stacked aggregates and that within these stacked systems they have certain arrangements in their aggregate forms.[85] However, it was discovered that van der Waals forces can also contribute to the intensity of the π-stacking but that they are not controlling the geometry of interaction. Within these structures they stated that, between two π-interaction systems, stability increases with an electron-rich (pyrrole) and electron-poor (pyridine) moiety exhibiting π-stacking; here the average π-stacking distance ranges from 3.3 to 3.8 Å.[89] Therefore, with these rules in mind, the most likely aggregate structures of 4-(pyrrol-1-yl)pyridine are shown in a simplified form in Scheme 1. Here, two monomers are utilized to illustrate the π-stacking, but the actual aggregate system is far larger.

In further considering the two aggregate structures, "face stacking" has been shown to exhibit hypochromism in solution as opposed to the "off-set" π-stacked system.[89] Knowing this, it is far more likely our 4-(pyrrol-1-yl)pyridine system exhibits "off-set" stacking. Further confirmation of an aggregate present is supported by the visible scattering at long wavelengths in the UV−visible spectrum of 4-(pyrrol-1-yl)pyridine and the increased intensity of the nitropyrrole-based final product absorbance at 509 nm, which is highlighted by a deep wine-red hue.

An estimate of approximately 400 to 1020 monomers for the 4-(pyrrol-1-yl)pyridine in solution is reached from the 142−363 nm size range indicated in Table 1 and the mean value of

Scheme 1. (A) "Face to face" π Stacking of 4-(Pyrrol-1-yl)pyridine with Average π Stacking Distance from Centroid to Centroid from Literature Values; (B) "Off-set" π Stacking of 4-(Pyrrol-1-yl)pyridine with Average π Stacking Distance from Centroid to Centroid from Literature Values[a]

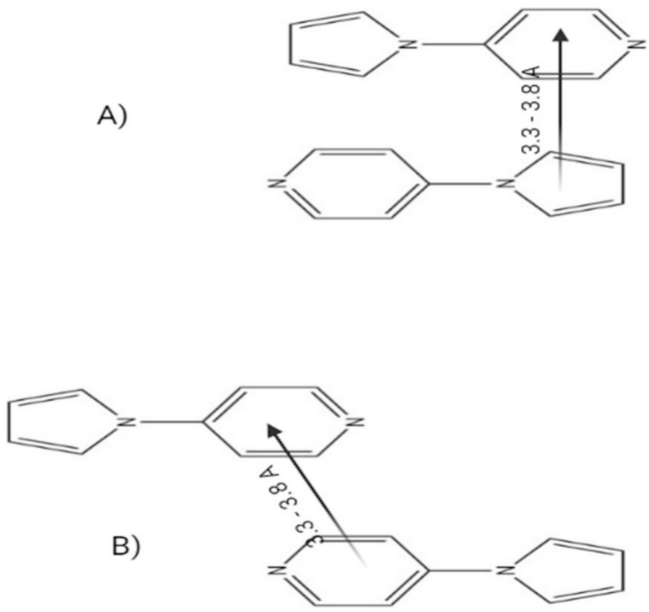

[a]Two moieties are illustrated to simplify the large aggregate system.

3.55 Å for the literature value of a centroid to centroid distance of the π-stacked system.[86] Moreover, the previously noted low molar absorptivity value of 110 M^{-1} cm^{-1} is consistent with an intermolecular $\pi \rightarrow \pi^*$ transition in this system.

As previously discussed, ^{1}H NMR of the 4-(pyrrol-1-yl)pyridine system exhibited downfield peak shifting and line broadening. The downfield shifting is indicative of intermolecular interactions in the system. However, the downfield shifting and broadening of only the pyridine protons and not the pyrrole protons further serve to prove the "off-set" stacking of the 4-(pyrrol-1-yl)pyridine aggregate. Here, no strong downfield shift of peak broadening would occur with the hydrogens on the pyrrole ring, as it is not actively participating in the π-stacking holding the aggregate together.

Computational studies are currently underway, although complicated by the supramolecular nature of this system. Additionally, the sensing properties of several derivatives of 4-(pyrrol-1-yl)pyridine are currently being pursued to provide greater insight into their mechanism of action.

Possible Commercial Advantages. Due to the high sensitivity (0.330 ppm) of the sensor to nitrite, this system serves to improve current methodology. For instance, as previously discussed, many current systems for nitrite detection have challenges. These range from tedious experimental procedures to increased reaction time, intensive mechanisms, pH limitations, and interference from other agents. By eliminating these complications, new methodology can be explored that still meet the required detection limits of both the EPA and WHO. The sensitivity of the sensor discussed here falls within the common range of LODs within the ppm or ppb range.[35−43]

The increased ease of detection, potential portability with a hand-held spectrometer, rapid response, and drastic colori-

https://doi.org/10.1021/acsomega.4c05026
ACS Omega 2024, 9, 37278−37287

metric change between the sensor and nitrite provide valuable advances into anion sensing. Additionally, the sensor's intricate aggregation ability provides insight into new mechanisms for anion sensing that can take advantage of supramolecular interactions causing increased sensitivity and selectivity to a target analyte of interest. This aspect is under further investigation, including studies of analogous aggregation based sensor systems.

CONCLUSION

In summary, with the synthesis of 4-(pyrrol-1-yl)pyridine we have discovered a new small-molecule colorimetric chemodosimeter for the detection of nitrite in aqueous solutions. Simple naked eye detection can be employed with the sensor system experiencing a color change from yellow to pink, and this reaction is irreversible and instantaneous. The mechanism of sensing is unusual, as it involves changes in the degree of aggregation in solution, subsequently affecting the extent of π-stacking and the intermolecular electronic transitions. This effectively amplifies the nitrite ion detection, resulting in an extremely low limit of detection of 0.330 ($\pm$0.09) ppm, and meets the criteria for the maximum contaminate levels from both the WHO and EPA. Overall, the sensor system may prove to be valuable for nitrite detection in the food industry, as it possesses several important features such as low cost, rapid testing, ease of analysis, high sensitivity, and high selectivity.

ASSOCIATED CONTENT

Supporting Information

The Supporting Information is available free of charge at https://pubs.acs.org/doi/10.1021/acsomega.4c05026.

^{1}H, ^{13}C, HSQC, and COSY NMR spectra of 4-(pyrrol-1-yl)pyridine at various concentrations in both d-DMSO and $CDCl_3$; ^{1}H and COSY NMR spectra of 4-(pyrrol-1-yl)pyridine with addition of nitrite ion PDF)

AUTHOR INFORMATION

Corresponding Author

Alistair J. Lees − *Department of Chemistry, Binghamton University, Binghamton, New York 13902-6000, United States;* orcid.org/0009-0007-0948-0169; Email: alees@binghamton.edu

Authors

Mallory E. Thomas − *Department of Chemistry, Binghamton University, Binghamton, New York 13902-6000, United States*

Lynn D. Schmitt − *Department of Chemistry, SUNY Cortland, Cortland, New York 13045, United States*

Complete contact information is available at: https://pubs.acs.org/10.1021/acsomega.4c05026

Author Contributions

M.E.T. conducted all the experimental work. All participated in the development of design and methodology. All performed data analysis. A.J.L. supervised the research project. M.E.T. and A.J.L. wrote the article, and all approved the final version of the manuscript.

Notes

The authors declare no competing financial interest.

ACKNOWLEDGMENTS

Funding was obtained from the Department of Chemistry and the Office of Entrepreneurship and Innovation Partnerships at Binghamton University. We thank Binghamton University faculty, Professors Susan Bane, Chuan-Jian Zhong, and Huiyuan Guo for access to instrumentation and Dr. Juergen Schulte for his valuable NMR expertise.

REFERENCES

(1) United States Environmental Protection Agency. *National Primary Drinking Water Regulations: Contaminant Specific Fact Sheets*; Inorganic Chemicals, Consumer Version: Washington, DC, 1995.

(2) Moorcroft, M. J.; Davis, J.; Compton, R. G. Detection and Determination of Nitrate and Nitrite: a review. *Talanta* **2001**, *54*, 785−803.

(3) Fanning, J. C. The Chemical Reduction of Nitrate in Aqueous Solution. *Coord. Chem. Rev.* **2000**, *199*, 159−179.

(4) Nollet, L. M. L. *Handbook of Water Analysis*, 2nd ed.; CRC Press: Boca Raton, FL, 2000; pp 1−784.

(5) *Guidelines for Drinking Water Quality*, 2nd ed. Addendum to Vol. *2*; Health criteria and other supporting information; World Health Organization: Geneva, 1998.

(6) Rajasulochana, P.; Ganesan, Y.; Kumar, P. S.; Mahalazmi, S.; Tasneem, F.; Ponnuchamy, M.; Kapoor, A. Paper-Based Microfluidic Colorimetric Sensor on a 3D Printed Support for Quantitative Detection of Nitrite in Aquatic Environments. *Environ. Res.* **2022**, *208*, 112745.

(7) Burt, T. P.; Howden, N. J. K.; Worral, F.; Whelan, M. J. Long-term monitoring of river water nitrate: how much data do we need? *J. Environ. Monit.* **2010**, *12*, 71−79.

(8) Carpenter, S. R.; Caraco, N. F.; Correll, D. L.; Howarth, R. W.; Sharpley, A. N.; Smit, V. H. Nonpoint pollution of surface waters with phosphorus and nitrogen. *Ecol. Appl.* **1998**, *8*, 559−568.

(9) Cameron, K. C.; Di, H. J.; Moir, J. L. Nitrogen losses from the soil/plant system: a review. *Ann. Appl. Biol.* **2013**, *162*, 145−173.

(10) Zia, H.; Harris, N. R.; Merrett, G. V.; Rivers, M.; Coles, N. The impact of agricultural activities on water quality: A case for collaborative catchment-scale management using integrated wireless sensor networks. *Comput. Electron. Agr.* **2013**, *96*, 126−138.

(11) Ahmad, R.; Ahn, M. S.; Hahn, Y. B. A highly sensitive nonenzymatic sensor based on Fe_2O_3 nanoparticle coated ZnO nanorods for electrochemical detection of nitrite. *Adv. Mater. Interfaces* **2017**, *4*, 1700691−1700700.

(12) Li, X. R.; Kong, F. Y.; Liu, J.; Liang, T. M.; Xu, J. J.; Chen, H. Y. Synthesis of Potassium-Modified Graphene and its Application in Nitrite-Selective Sensing. *Adv. Funct. Mater.* **2012**, *22*, 1981−1988.

(13) Ye, D.; Luo, L.; Chen, Q.; Liu, X. A novel nitrite sensor based on graphene/polypyrrole/chitosan nanocomposite modified glassy carbon electrode. *Analyst* **2011**, *136*, 4563−4569.

(14) Zuane, J. D. Handbook of Drinking Water Quality, 2nd edn.: Wiley, New York, NY, 1996; pp 1−592.

(15) Zhang, L.; Huang, J.; Hu, Z.; Li, X.; Ding, T.; Hou, X.; Chen, Z.; Ye, Z.; Luo, R. $Ni(NO_3)^{2-}$ induced high electrocatalytic hydrogen evolution performance of self-supported fold like WC coating on carbon fiber paper prepared through molten salt method. *Electrochem. Acta* **2022**, *422*, 140553.

(16) Zhe, T.; Li, R.; Li, F.; Liang, S.; Shi, D.; Sun, X.; Liu, Y.; Cao, Y.; Bu, T.; Want, L. Surface Engineering of Carbon Selenide Nanofilms on Carbon Cloth: An Advanced and Ultrasensitive Self-Supporting Binder-Free Electrode for Nitrite Sensing. *Food Chem.* **2021**, *340*, 127953.

(17) Sihto, H. M.; Budi Susila, Y.; Tasara, T.; Radstrom, P.; Stephan, R.; Schelin, J.; Johler, S. Effect of Sodium Nitrite and Regulatory Mutations Δagr, ΔsarA, and ΔsigB on the MRNA and Protein Levels of Staphylococcal Enteroxtoxin. *Food Control.* **2016**, *65*, 37−45.

(18) Akyuz, M.; Ata, S. Determination of Low-Level Nitrite and Nitrate in Biological, Food, and Environmental Samples by Gas

Chromatography-Mass spectrometry and Liquid Chromatography with Fluorescence Detection. *Talanta* **2009**, *79*, 900−904.
(19) Hospital, X. F.; Hierro, E.; Arnau, J.; Carballo, J.; Aguirre, J. S.; Gratacos-Cubarsi, M.; Fernandex, M. Effect of Nitrate and Nitrite on Listeria and Selected Spoilage Bacteria Inoculated in Dry-Cured Ham. *Food. Res. Int.* **2017**, *101*, 82−87.
(20) Abdulmumeen, H. A.; Risikat, A. N.; Sururah, A. R. Food: its preservatives, additives, and applications. *Int. J. Chem. Biochem. Sci.* **2012**, *1*, 36−47.
(21) Chen, X.; Chen, X.; Zhu, L.; Liu, W.; Jiang, L. Programming an orthogonal self-assembling protein cascade based on reactive peptide-protein pairs for in vitro enzymatic trehalose production. *J. Agric. Food Chem.* **2022**, *70*, 4690−4700.
(22) Larson, S. C.; Bergkvist, L.; Wolk, A. Processed Meat Consumption, Dietary Nitrosamines and Stomach Cancer Risk in a Cohort of Swedish Women. *Int. J. Cancer* **2006**, *119*, 915−919.
(23) Neth, M. R.; Love, J. S.; Horowitz, B. Z.; Shertz, M. D.; Sahni, R.; Daya, M. R. Fatal sodium nitrite poisoning: key considerations for prehospital providers. *Prehosp. Emerg. Care.* **2021**, *25*, 844−850.
(24) Manassaram, D. M.; Backer, L. C.; Moll, D. M. A Review of Nitrates in Drinking Water: Maternal Exposure and Adverse Reproductive and Developmental Outcomes. *Environ. Health Perspect.* **2006**, *114*, 320−324.
(25) Bryan, N. S.; Fernandez, B. O.; Bauer, S. M.; Garcia-Saura, M. F.; Milson, A. B.; Rassaf, T.; Maloney, R. E.; Bharti, A.; Rodriguez, J.; Feelisch, M. Nitrite is a Signalling Molecule and Regulator of Gener Expression in Mammalian Tissues. *Nat. Chem. Biol.* **2005**, *1*, 290−297.
(26) Ye, D.; Luo, L.; Ding, Y.; Chen, Q.; Liu, X. Synthesis of Potassium-Modified Graphene and its Application in Nitrite-Selective Sensing. *Analyst* **2011**, *136*, 4563−4569.
(27) Song, P.; Wu, L.; Guan, W. Dietary nitrates, nitrites, and nitrosamines intake and the risk of gastric cancer: a meta-analysis. *Nutrients* **2015**, *7*, 9872−9895.
(28) Balimandawa, M.; de Meester, C.; Leonard, A. The mutagenicity of nitrite in the Salmonella/microsome test system. *Mutat. Res. Genet. Toxicol.* **1994**, *321*, 7−11.
(29) Ma, L.; Hu, L.; Feng, X.; Wang, S. Nitrate and Nitrite in Health and Disease. *Aging Dis.* **2018**, *9*, 938−945.
(30) Shepard, S. E. Endogenous formation of N-nitroso compounds in relation to the intake of nitrate or nitrite. In: Health aspects of nitrate and its metabolites. *Food Chem. Toxicol.* **1995**, *30*, 137−150.
(31) Fan, A. M.; Steinberg, V. E. Health implications of nitrate and nitrite in drinking water: an update on methemoglobinemia occurrence and reproductive and developmental toxicity. *Regul. Toxicol. Pharmacol.* **1996**, *23*, 35−43.
(32) Puangpila, C.; Jakmunee, J.; Pencharee, S.; Pensrisirikul, W. Mobile-phone based colorimetric analysis for determining nitrite content in water. *Environ. Chem.* **2018**, *15*, 403−410.
(33) Ward, M. H.; Mark, S. D.; Cantor, K. P.; Weisenburger, D. D.; Correa-Villasenor, A.; Zahm, S. H. Drinking Water Nitrate and the Risk of Non-Hodgkin's Lymphoma. *Epidemiology* **1996**, *7*, 465−471.
(34) World Health Organization. *Nitrate and Nitrite in Drinking Water Background Document for Development of Drink Water*; **2009**, *2*, 21.
(35) Bagheri, H.; Hajian, A.; Rezaei, M.; Shirzadmehr, A. Composite of Cu metal nanoparticles-multiwall carbon nanotubes-reduced graphene oxide as a novel and high-performance platform of the electrochemical sensor for simultaneous determination of nitrite and nitrate. *J. Hazard. Mater.* **2017**, *324*, 762−772.
(36) Li, Y.; Zhang, X.; Sun, Y.; Yang, Z.; Liu, J. Fabrication Non-Enzymatic Electrochemical Sensor Based on Methyl Red and Graphene Oxide Nanocomposite Modified Carbon Paste Electrode for Determination of Nitrite in Food Samples. *Int. J. Electrochem. Sci.* **2023**, *18*, 100097.
(37) Nussler, A. K.; Glanemann, M.; Schirmeier, A.; Liu, L.; Nussler, N. C. Fluorometric measurement of nitrite/nitrate by 2,3-diaminonaphthalene. *Nat. Protoc.* **2006**, *1*, 2223−2226.
(38) Ohta, T.; Arai, Y.; Takitani, S. Fluorometric determination of nitrite with 4-hydroxycoumarin. *Anal. Chem.* **1986**, *58*, 3132−3135.
(39) Adarsh, N.; Shanmugasundaram, M.; Ramaiah, D. Efficient Reaction Based Colorimetric Probe for Sensitive Detection, Quantification, and on-Site Analysis of Nitrite Ions in Natural Water Resources. *Anal. Chem.* **2013**, *85*, 10008−10012.
(40) Singh, L.; Ranjan, N. Highly Selective and Sensitive Detection of Nitrite Ion by an Unusual Nitration of a Fluorescent Benzimidazole. *J. Am. Chem. Soc.* **2023**, *145*, 2745−2749.
(41) Shou, Y.; Yan, D.; Wei, M. A 2D quantum-dot based electrochemiluminescence film sensor towards reversible temperature-sensitive response and nitrite detection. *J. Mater. Chem.* **2015**, *3*, 10099−10106.
(42) Garside, C. A chemiluminescent technique for the determination of nanomolar concentrations of nitrate and nitrite in seawater. *Mar. Chem.* **1982**, *11*, 159−167.
(43) Chen, H.; Fang, Y.; An, T.; Zhu, K.; Lu, J. Simultaneous spectrophotometric determination of nitrite and nitrate in water samples by flow-injection analysis. *Int. J. Environ. Anal. Chem.* **2000**, *76*, 89−98.
(44) European Standard. European Standard. Water quality determination of nitrites molecular absorption spectrometric method; 1993.
(45) Fox, J. B. Kinetics and Mechanisms of the Greiss Reaction. *J. Anal. Biochem.* **1979**, *51*, 1493.
(46) Guembe-Garcia, M.; Gonzalez-Ceballos, L.; Arnaiz, A.; Fernandez-Muino, M. A.; Sancho, M. T.; Oses, S. M.; Ibeas, S.; Rovira, J.; Melero, B.; Represa, C.; Garcia, J. M.; Vallejos, S. Easy Nitrite Analysis of Processed Meat with Colorimetric Polymer Sensors and a Smartphone App. *ACS Appl. Mater. Interfaces* **2022**, *14*, 37051−37058.
(47) Zhao, W.; Yang, H.; Xu, S.; Li, X.; Wei, W.; Liu, X. Olive-Structured" Nanocomposite Based on Environmental Nitrite Detection. *ACS Sustain. Chem. Eng.* **2019**, *7*, 17424−17431.
(48) Lin, B.; Xu, J.; Lin, K.; Li, M.; Lu, M. Low-Cost Automatic Sensor for In Situ Colorimetric Detection of Phosphate and Nitrite in Agricultural Water. *ACS Sens.* **2018**, *3*, 2541−2549.
(49) Gu, Z.; Wu, M. L.; Yan, B. Y.; Wang, H. F.; Kong, C. Integrated Digital Microfluidic Platform for Colorimetric Sensing of Nitrite. *ACS Omega* **2020**, *5*, 11196−11201.
(50) Singh, P.; Singh, M. K.; Beg, Y. R.; Nishad, G. R. A review on spectroscopic methods for determination of nitrite and nitrate in environmental samples. *Talanta* **2019**, *191*, 364−381.
(51) Seki, K.; Ohkura, K.; Terashima, N.; Kanaoka, Y. Photoreaction of 4-iodopyridine with Herteroaromatics. *Heterocycles* **1986**, *24*, 799.
(52) Barckholtz, C.; Barckholz, T. A.; Hadad, C. M. C-H and N-H Bond Dissociation Energies of Small Aromatic Hydrocarbons. *J. Am. Chem. Soc.* **1999**, *121*, 491−500.
(53) Schmitt, L.; Lees, A. J.; US 2020/0363382, 2020.
(54) Chen, H.; Wang, Q.; Tao, F. A Novel Palladium-catalyzed Amination of aryl Halides with Amines using rac-P-Phos as the Ligand. *Chin. J. Chem.* **2009**, *27*, 1382−1386.
(55) Pai, G.; Asoke, P. C. Ligand-free Copper Nanoparticle promoted N-arylation of azoles with aryl and heteroaryl iodides. *Tetrahedron Lett.* **2014**, *55*, 941−944.
(56) Teo, Y. C.; Yong, F. F.; Sim, S. Ligand-free Cu_2O-catalyzed cross coupling of nitrogen heterocycles with iodopyridines. *Tetrahedron* **2013**, *69*, 7279−7284.
(57) Abraham, R. J.; Berstein, H. J. The Proton Resonance Spectra of Furan and Pyrrole. *Can. J. Chem.* **1959**, *37*, 1056−1065.
(58) Iwaszuk, A.; Lucid, A. K.; Kazeeb, K. M.; Nolan, M. First principles investigation of anion-controlled red shift in light absorption in ZnX (X = O, S, Se) nanocluster modified rutile TiO_2. *J. Mater. Chem. A* **2014**, *2*, 18796.
(59) Nakagawa, R.; Evanisto de Sousa, L.; Tohnai, N.; Minakata, S.; de Silva, P.; Takeda, Y. Anion-Responsive Colorimetric and Fluorometric Red-Shift in a Triarylborane Derivative: Dual Role of Phenazoborine as a Lewis Acid and Electron Donor. *Angew. Chem.* **2024**, *63*, No. e202405158.

https://doi.org/10.1021/acsomega.4c05026
ACS Omega 2024, 9, 37278−37287

(60) Liao, X.; Fang, J.-A.; Zhao, J.-L.; Ruan, Q.; Zeng, X.; Luo, Q.-Y.; Redshaw, C. An efficient ICT-based ratio/colorimetric tripodal azobenzene probe for the recognition/discrimination of F^-, AcO^-, and $H_2PO_4^-$ anions. *Spectr. Chim. Acta. Part A* **2019**, *221*, 117174.
(61) Tsujimura, M.; Noji, T.; Saito, K.; Sudo, Y. Mechanism of absorption wavelength shifts in anion channelrhodopsin-1 mutants. *BBA-Bioenergetics* **2021**, *1862*, 148349.
(62) Schmalzbauer, M.; Marcon, M.; Konig, B. Excited State Anions in Organic Transformations. *Angew. Chem, Int. Ed.* **2021**, *60*, 6270−6292.
(63) Li, Z.; Wu, F.-Y.; Guo, L.; Li, A.-F.; Jiang, Y.-B. Enhanced Anion Binding of N-(Anilino)thioureas. Contribution of the N-Anilino -NH Proton Acidity. *J. Phys. Chem. B* **2008**, *112*, 7071−7079.
(64) Zhang, R.; Duan, N.; Jiang, L.; Xu, F.; Cheng, W.; Zhu, G.; Gao, W. Electronic Excitation Characteristics and Spectral Behavior of Phosphate Anions. *Langmuir* **2023**, *39*, 9411−9153.
(65) Trampuz, M.; Znidanc, M.; Gallou, F.; Casar, Z. Does the Red Shift in UV-Vis Spectra Really Provide a Sensing Option for Detection of N-nitrosamines Using Metalloporphyrins? *ACS Omega* **2023**, *8*, 1154−1167.
(66) Zhao, L.; Ren, Z.; Yan, X. Assembly Induced Super-Large Red-Shifted Absorption: The Burgeoning Field of Organic Near-Infrared Materials. *CCS Chem.* **2021**, *3*, 678−693.
(67) Shedge, S. P.; Zuehlsdorff, T. J.; Servis, M. J.; Clark, A. E.; Isborn, C. M. Effect of Ions on the Optical Absorption Spectra of Aqueously Solvated Chromophores. *J. Phys. Chem.A* **2019**, *123*, 6175−6184.
(68) Ding, X. B.; Brimble, M. A.; Furkert, D. P. Reactivity of 2-Nitropyrrole Systems: Development of Improved Synthetic Approaches to Nitropyrrole Natural Products. *J. Org. Chem.* **2018**, *83*, 12460−12470.
(69) Morgan, K. J.; Morrey, D. P. Nitropyrroles-I. *Tetrahedron* **1966**, *22*, 57−62.
(70) Hills, B. P.; Takacs, S. F.; Belton, P. S. The Effects of Proteins on the Proton N.M.R. Transverse Relaxation Time of Water. *Mol. Phys.* **1989**, *67*, 919−937.
(71) McGarrity, J. F.; Ogle, C. A. High-Field Proton NMR Study of the Aggregation and Complexation of N-Butyllithium in Tetrahydrofuran. *J. Am. Chem. Soc.* **1985**, *107*, 1805−1810.
(72) Okazawa, N.; Sorensen, T. S. The Line-Shape Analysis of Nuclear Magnetic Resonance Peaks Broadened by the Presence of a "hidden" Exchange Partner. *Can. J. Chem.* **1978**, *56*, 2737−2742.
(73) Imbardelli, D.; Chidichiomo, G.; Longeri, M. Nuclear Relaxation of Partially Oriented Pyridine Determined by Line Width Analysis of ^{1}H NMR Spectra. *Chem. Phys. Lett.* **1987**, *135*, 319−324.
(74) Parteni, F.; Tassinari, F.; Libertini, E.; Lanzi, M.; Mucci, A. π-Stacking Signature in NMR Solution Spectra of Thiophene-Based Conjugated Polymers. *ACS Omega* **2017**, *2*, 5775−5784.
(75) Gjuroski, I.; Furrer, J.; Vermathen, M. Probing the Interactions of Porphyrins with Macromolecules using NMR Spectroscopy Techniques. *Molecules* **2021**, *26*, 1942−1985.
(76) Becker, E.; Bradley, R. Effects of "Ring Currents" on the NMR Spectra of Porphyrins. *J. Chem. Phys.* **1959**, *31*, 1413−1414.
(77) Jerlov, N. G.; Kullenber, B. The Tyndall Effect of Uniform Minerogenic Suspensions. *Tellus* **1953**, *5*, 306−307.
(78) Xiao, W.; Deng, Z.; Huang, Z.; Zhuang, M.; Yuan, Y.; Nie, J.; Zhang, Y. Highly Sensitive Colorimetric Detection of a Variety of Analytes via the Tyndall Effect. *Anal. Chem.* **2019**, *91*, 15114−15122.
(79) Bender, M. The Use of Light Scattering for Determining Particle Size and Molecular Weight and Shape. *J. Chem. Educ.* **1952**, *29*, 15.
(80) Kanjanawarut, R.; Yuan, B.; Xiano, D. S. UV-Vis Spectroscopy and Dynamic Light Scattering Study of Gold Nanorods Aggregation. *Nucleic Acid Ther.* **2013**, *23*, 273−280.
(81) Duff, D. G.; Kirkwood, D. J.; Stevenson, D. M. The Behaviour of Dyes in Aqueous Solutions. I. The Influence of Chemical Structure on Dye Aggregation a Polarographic Study. *J. Soc. Dyes. Colour* **1977**, *93*, 303−306.
(82) Navarro, A.; Sanz, F. Dye aggregation in solution: Study of C.I. direct red I. *Dyes Pigments* **1999**, *40*, 131−139.
(83) Martinez-Manez, R.; Sancenon, F. Fluorogenic and Chromogenic Chemosensors, and Reagents for Anions. *Chem. Rev.* **2003**, *103*, 4419−4476.
(84) Yu, H.; Aziz, H. Direct Observation of Exciton-Induced Molecular Aggregation in Organic Small-Molecule Electroluminescent Materials. *J. Phys. Chem. C* **2019**, *123*, 16424−16429.
(85) Gao, M.; Tang, B. Z. Fluorescent Sensors Based on Aggregation-Induced Emission: Recent Advances and Perspectives. *ACS Sens.* **2017**, *2*, 1382−1399.
(86) Graham, D. J. Information Content in Organic Molecules: Aggregation States and Solvent Effects. *J. Chem. Inf. Model.* **2005**, *45*, 1223−1236.
(87) Martinez, C. R.; Iverson, B. L. Rethinking the Term "Pi-Stacking. *Chem. Sci.* **2012**, *3*, 2191.
(88) Hunter, C. A.; Sanders, J. K. The Nature of Pi-Pi Interactions. *J. Am. Chem. Soc.* **1990**, *112*, 5525−5534.
(89) Janiak, C. A Critical Account on π-π Stacking in Metal Complexes with Aromatic Nitrogen-Containing Ligands. *J. Chem. Soc.* **2000**, *21*, 3885−3896.

https://doi.org/10.1021/acsomega.4c05026
ACS Omega 2024, 9, 37278−37287